

# Entanglement phase transitions in non-Hermitian quasicrystals

Longwen Zhou<sup>1,2,3,\*</sup>

<sup>1</sup>*College of Physics and Optoelectronic Engineering,  
Ocean University of China, Qingdao, China 266100*

<sup>2</sup>*Key Laboratory of Optics and Optoelectronics, Qingdao, China 266100*

<sup>3</sup>*Engineering Research Center of Advanced Marine Physical Instruments and Equipment of MOE, Qingdao, China 266100*

(Dated: 2024-01-18)

The scaling law of entanglement entropy could undergo qualitative changes during the nonunitary evolution of a quantum many-body system. In this work, we uncover such entanglement phase transitions for free fermions in one-dimensional non-Hermitian quasicrystals (NHQCs). We identify two types of entanglement transitions with different scaling laws and critical behaviors due to the interplay between non-Hermitian effects and quasiperiodic potentials. The first type represents a typical volume-law to area-law transition, which happens together with a PT-symmetry breaking and a localization transition. The second type features an abnormal log-law to area-law transition, which is mediated by a critical phase with a volume-law scaling in the steady-state entanglement entropy. These entangling phases and transitions are demonstrated in two representative models of noninteracting NHQCs. Our results thus advanced the study of entanglement transitions in non-Hermitian disordered systems and further disclosed the rich entanglement patterns in NHQCs.

## I. INTRODUCTION

Along with the increase of measurement rates, the competition between unitary time evolution and projective measurements could prompt the steady state of a quantum many-body system (either interacting or non-interacting) to switch from a volume-law-entangled phase to a quantum Zeno phase with an area-law entanglement entropy (EE) [1–5]. Ever since its discovery, this measurement-induced entanglement phase transition has attracted great attention in both theoretical [6–52] and experimental [53–55] studies, with important implications for the understanding of quantum information dynamics and the simulation of quantum many-body systems [56–58]. Recently, entanglement phase transitions are also studied in the context of non-Hermitian physics [59–66]. There, the effect of measurement is taken into account by considering a nonunitary evolution generated by a non-Hermitian Hamiltonian. The dissipation-gap formation and the non-Hermitian skin effect are further identified as two typical mechanisms of producing entangling-disentangling phase transitions [62, 63]. Yet, these discoveries are established with a focus on pristine non-Hermitian lattice models.

Non-Hermitian quasicrystal (NHQC) forms a typical category of disordered non-Hermitian setup [67–69]. In an NHQC, the interplay between correlated disorder and gain/loss or nonreciprocal effects could yield rich phases and phenomena including parity-time-reversal-(PT-) symmetry breaking transitions, localization transitions, topological transitions and mobility edges [70–75]. Despite great theoretical efforts [76–107], NHQCs have also been experimentally realized by nonunitary photonic quantum walks [108, 109]. However, much less

is known regarding entanglement phase transitions in NHQCs [104, 105]. This question can be interesting, as a PT-broken NHQC could belong to either a localized phase [71] or an extended phase [70]. In the latter case, the delocalized bulk states should prefer a volume-law scaling in the steady-state EE after a long-time evolution, while the dissipation gap in the complex energy spectrum may favor an area-law entanglement scaling. The competition between these two opposite trends may lead to new scaling laws and exotic critical behaviors for the EE. Moreover, an NHQC could possess a point-gap instead of a line-gap on the complex energy plane [70, 71], and the implication of a point dissipation gap on entanglement phase transitions is largely unclear. Besides, whether and how entanglement transitions would accompany other phase transitions (e.g., PT-symmetry breaking, localization, etc.) in NHQCs remain to be uncovered.

To resolve these puzzles, we explore in this work the entanglement phase transitions of free fermions in NHQCs, with a focus on two “minimal” and mutually dual non-Hermitian lattice models [72, 79]. In Sec. II, we introduce these models and review their known spectral and localization properties. The entanglement phase transitions in these models are explored in detail in Sec. III. A unique type of log-law to area-law entanglement transition, mediated by a volume-law critical entangling phase is identified. In Sec. IV, we summarize our results, comment on related issues and discuss potential future directions.

## II. MODELS

We focus on the entanglement phase transitions in two “minimal” non-Hermitian variants of the noninteracting Aubry-André-Harper (AAH) model. They will be denoted by NHAH1 and NHAH2 for brevity. We first go over some of their key physical properties in this sec-

\* zhoulw13@u.nus.edu

tion. Throughout the discussions, we will set the lattice constant  $a = 1$  and the Planck constant  $\hbar = 1$ .

In the position representation, the Hamiltonian of the NHA AH1 takes the form of

$$\hat{H}_1 = J \sum_n (\hat{c}_n^\dagger \hat{c}_{n+1} + \hat{c}_{n+1}^\dagger \hat{c}_n) + V \sum_n e^{-i2\pi\alpha n} \hat{c}_n^\dagger \hat{c}_n. \quad (1)$$

Here  $\hat{c}_n^\dagger$  ( $\hat{c}_n$ ) creates (annihilates) a fermion on the lattice site  $n$ .  $J$  denotes the nearest-neighbor hopping amplitude and  $V$  denotes the amplitude of onsite potential  $V_n = V e^{-i2\pi\alpha n}$ .  $2\pi\alpha$  describes the wavenumber of the superlattice [110]. Expanding a general state as  $|\psi\rangle = \sum_n \psi_n \hat{c}_n^\dagger |\emptyset\rangle$ , the eigenvalue equation  $\hat{H}_1 |\psi\rangle = E |\psi\rangle$  of NHA AH1 can be expressed in the following form

$$J\psi_{n+1} + J\psi_{n-1} + V e^{-i2\pi\alpha n} \psi_n = E \psi_n. \quad (2)$$

Here  $|\emptyset\rangle$  denotes the vacuum state and the amplitude  $\psi_n$  is normalized as  $\sum_n |\psi_n|^2 = 1$ . It is clear that the NHA AH1 is non-Hermitian due to the complex onsite phase factor  $e^{-i2\pi\alpha n}$ . It further possesses the PT symmetry, with the parity  $\mathcal{P} : n \rightarrow -n$  and the time-reversal  $\mathcal{T} = \mathcal{K}$ , where  $\mathcal{K}$  performs the complex conjugation. The quasicrystal nature of the system comes about by setting  $\alpha$  as an irrational number, so that the onsite potential is spatially quasiperiodic. The energy spectrum of the system under the periodic boundary condition (PBC) was found to take the conjectured form of [72]

$$E = \begin{cases} 2J \cos k & |V| \leq |J| \\ \left(V + \frac{J^2}{V}\right) \cos k + i \left(V - \frac{J^2}{V}\right) \sin k & |V| > |J| \end{cases}. \quad (3)$$

Here  $k \in [-\pi, \pi)$  is an artificial parameter that tells us the eigenenergies either fill the region of a line segment or an ellipse [111]. Therefore, the spectrum is real for  $|V| < |J|$  (PT-invariant) and complex for  $|V| > |J|$  (PT-broken). There is a PT transition in the energy spectrum at  $|V| = |J|$ .

The Hamiltonian of the NHA AH2 in the position representation is given by

$$\hat{H}_2 = J \sum_n \hat{c}_{n+1}^\dagger \hat{c}_n + 2V \sum_n \cos(2\pi\alpha n) \hat{c}_n^\dagger \hat{c}_n, \quad (4)$$

and the related eigenvalue equation reads

$$J\psi_{n-1} + 2V \cos(2\pi\alpha n) \psi_n = E \psi_n. \quad (5)$$

It is clear that the nearest-neighbor hopping is unidirectional from left to right, making the system non-Hermitian. The NHA AH1 and NHA AH2 differ in both their hopping and onsite potential terms, so that neither of them can be viewed as a special case of the other. The NHA AH2 is also quasiperiodic if  $\alpha$  is irrational [110]. Taking a rational approximation for  $\alpha \simeq p/q$  (with  $p, q$  being co-prime integers) and performing the discrete Fourier transformation  $\psi_n = \frac{1}{L} \sum_{\ell=1}^L \phi_\ell e^{i2\pi\alpha n}$

under the PBC ( $\psi_n = \psi_{n+L}$ ), the Eq. (5) can be transformed to the momentum space [71] as

$$V\phi_{\ell+1} + V\phi_{\ell-1} + J e^{-i2\pi\alpha\ell} \phi_\ell = E \phi_\ell, \quad (6)$$

where  $L$  denotes the length of lattice. It is now clear that the NHA AH2 also possesses the PT symmetry, with  $\mathcal{P} : \ell \rightarrow -\ell$  and  $\mathcal{T} = \mathcal{K}$ . The energy spectrum of the system under the PBC is further given by the conjectured expression

$$E = \begin{cases} \left(J + \frac{V^2}{J}\right) \cos k + i \left(J - \frac{V^2}{J}\right) \sin k & |V| < |J| \\ 2V \cos k & |V| \geq |J| \end{cases}, \quad (7)$$

where  $k \in [-\pi, \pi)$  is again an artificial parameter [111]. Therefore, the spectrum is real for  $|V| > |J|$  (PT-invariant) and complex for  $|V| < |J|$  (PT-broken). The PT transition of NHA AH2 also happens at  $|V| = |J|$  [79].

By comparing the Eqs. (2) and (6), we further observe a duality relation between the NHA AH1 and NHA AH2, implying the presence of a fixed point along  $|J| = |V|$ . In fact, it has been identified that under the PBC and for any irrational  $\alpha$ , there is a PT spectral transition together with a localization-delocalization transition at  $|J| = |V|$  for both the NHA AH1 and NHA AH2. When  $|V| < |J|$ , the NHA AH1 (NHA AH2) resides in an extended phase with a real (complex) spectrum and holding only extended eigenstates. When  $|V| > |J|$ , the NHA AH1 (NHA AH2) switches to a localized phase with a complex (real) spectrum and holding only localized eigenstates [72, 79]. The transitions between these phases could be further captured by quantized changes of spectral topological winding numbers [70, 71].

In Fig. 1, we illustrate the phases and transitions in NHA AH1 and NHA AH2 by investigating their spectra and inverse participation ratios (IPRs). The  $\langle \text{Im}E \rangle$  [in Figs. 1(a) and 1(c)] and  $\langle \text{IPR} \rangle$  [in Figs. 1(b) and 1(d)] are defined as

$$\langle \text{Im}E \rangle = \frac{1}{L} \sum_{j=1}^L |\text{Im}E_j|, \quad (8)$$

$$\langle \text{IPR} \rangle = \frac{1}{L} \sum_{j=1}^L \sum_{n=1}^L |\psi_n^j|^4. \quad (9)$$

Here  $E_j$  is the  $j$ th eigenenergy of  $\hat{H}_1$  or  $\hat{H}_2$  with the normalized right eigenvector  $|\psi_j\rangle = \sum_{n=1}^L \psi_n^j \hat{c}_n^\dagger |\emptyset\rangle$ . By definition, we expect  $\langle \text{Im}E \rangle = 0$  ( $\langle \text{Im}E \rangle > 0$ ) in the PT-invariant (PT-broken) phase, and  $\langle \text{IPR} \rangle \rightarrow 0$  ( $\langle \text{IPR} \rangle > 0$ ) in the extended (localized) phase. The numerical results presented in Fig. 1 clearly verified the theoretically predicted extended/localized phases, PT transitions and localization transitions in these NHQCs [72, 79].

Based on these known physical properties, one may expect to have entanglement phase transitions also in

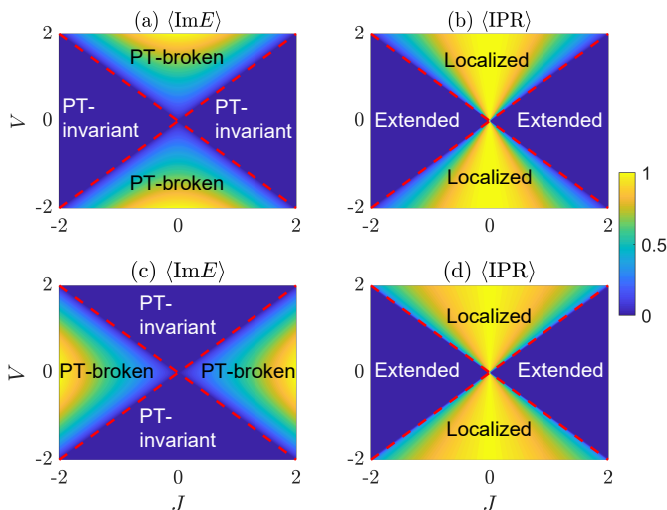


FIG. 1. Phase diagrams of the NHAH1 [in (a), (b)] and NHAH2 [in (c), (d)] under the PBC [112]. We choose  $\alpha = \frac{\sqrt{5}-1}{2}$  and the length of lattice  $L = 610$  for all panels. The red dashed lines show the phase boundaries  $J = \pm V$ . The NHAH1 stays in a PT-invariant extended phase for  $|V| < |J|$  and goes to a PT-broken localized phase for  $|V| > |J|$ . The NHAH2 resides in a PT-broken extended phase for  $|V| < |J|$  and switches to a PT-invariant localized phase for  $|V| > |J|$ .

the NHAH1 and NHAH2. For example, after a long-time evolution, the EE of a typical initial state might be proportional to the system size (volume-law) in the PT-invariant phase and become almost independent to the system size in the PT-broken phase (area-law) [63]. The PT transition of NHAH1 or NHAH2 should then accompany a volume-law to area-law entanglement transition. Meanwhile, one may also expect the scaling of steady-state EE to follow a volume-law in the extended phase and an area-law in the localized phase. However, the PT-invariant (PT-broken) phase of our system could also be a localized (an extended) phase, making the real physical situation more complicated. As will be demonstrated in the following section, despite the more conventional volume-law to area-law entanglement transitions, the steady-state EE of an NHQC may follow an abnormal log-law scaling due to the interplay between quasiperiodicity and non-Hermitian effects. A log-law to area-law entanglement phase transition could further be induced to happen across a critical point where the EE follows a volume-law.

### III. RESULTS

In this section, we reveal the entanglement phase transitions in NHAH1 and NHAH2. We first discuss the definition of EE and the calculation of its dynamics for a non-Hermitian system. Next, we demonstrate the scaling relations of steady-state EE with respect to the system and subsystem sizes for our two NHQC models in

Secs. III A and III B. These relations allow us to clearly distinguish different entangling phases in the considered systems. The entanglement phase transitions are further uncovered by investigating the changes of EE with respect to different system parameters. With all these information, we finally establish the entanglement phase diagrams for our NHQC models.

For a system consists of noninteracting fermions, the EE of an arbitrary subsystem and its time evolution can be extracted from the spectrum and dynamics of the single-particle correlator. Consider a system described by the quadratic Hamiltonian  $\hat{H} = \sum_{m,n} \hat{c}_m^\dagger H_{mn} \hat{c}_n$  and prepared at time  $t = 0$  in the initial state  $|\Psi_0\rangle$ , the normalized state of the system at a later time  $t$  is given by

$$|\Psi(t)\rangle = \frac{e^{-i\hat{H}t}|\Psi_0\rangle}{\sqrt{\langle\Psi_0|e^{i\hat{H}^\dagger t}e^{-i\hat{H}t}|\Psi_0\rangle}}. \quad (10)$$

Here  $\hat{c}_m^\dagger$  ( $\hat{c}_n$ ) creates (annihilates) a fermion at the lattice site  $m$  ( $n$ ). Note that for a non-Hermitian system, we generally have  $\hat{H} \neq \hat{H}^\dagger$ , leading to a nonunitary time evolution. In our calculations, we choose the initial state to be in the form of a charge density wave for a half-filled lattice, i.e.,

$$|\Psi_0\rangle = \prod_{r \in \mathbb{Z}} \hat{c}_{2r}^\dagger |\emptyset\rangle, \quad (11)$$

where  $r = 1, 2, \dots, \lfloor L/2 \rfloor - 1, \lfloor L/2 \rfloor$ . Other kinds of pure initial states generate similar results regarding the (sub)system-size scaling of steady-state EE. At a later time  $t$ , the element of single-particle correlation matrix  $C(t)$  in position representation is given by

$$C_{mn}(t) = \langle\Psi(t)|\hat{c}_m^\dagger \hat{c}_n|\Psi(t)\rangle, \quad (12)$$

Restricting the indices  $m$  and  $n$  to a subsystem A of size  $l$  and diagonalizing the corresponding  $l \times l$  block of  $C(t)$  result in the correlation-matrix spectrum  $\{\zeta_j(t)|j = 1, \dots, l\}$ . The EE at time  $t$  can then be obtained as [62]

$$S(t) = -\sum_{j=1}^l [\zeta_j(t) \ln \zeta_j(t) + (1 - \zeta_j(t)) \ln(1 - \zeta_j(t))]. \quad (13)$$

Note that the  $S(t)$  here is the bipartite EE of a subsystem A. It is defined by tracing over all the degrees of freedom belonging to a complementary subsystem B of the size  $L - l$ , in the sense that  $S = -\text{Tr}(\rho_A \ln \rho_A)$  and  $\rho_A = \text{Tr}_B(|\Psi(t)\rangle\langle\Psi(t)|)$ . Numerically, the EE of a Gaussian state can be computed efficiently following the recipe listed in the Appendix B of Ref. [62].

In the following subsections, we study the EE of our two NHQC models with the method outlined here. We focus on systems under the PBC and set the irrational parameter  $\alpha = (\sqrt{5} - 1)/2$  (the inverse golden ratio) for all our calculations. Other choices of the irrational  $\alpha$  lead to similar results.

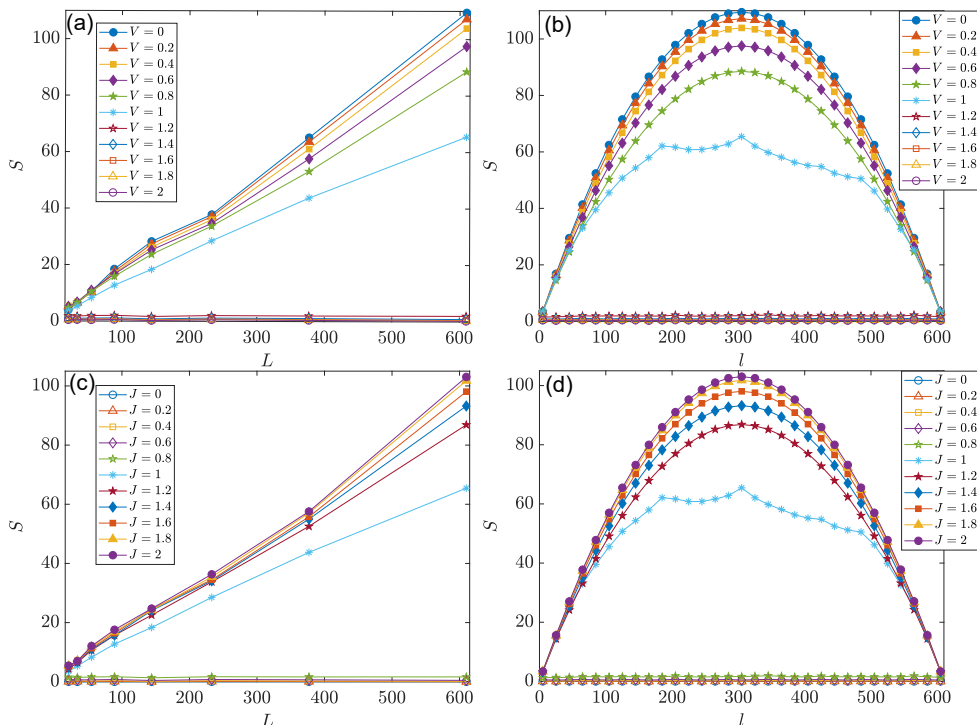


FIG. 2. Steady-state EE of the NHA AH1 at half-filling versus the system size  $L$  [under bi-partition in (a), (c)] and the subsystem size  $l$  [under a fixed length of lattice  $L = 610$  in (b), (d)]. Other system parameters are set as  $J = 1$  for (a), (b) and  $V = 1$  for (c), (d). The time span of the entire evolution is  $T = 1000$  [113].

### A. NHA AH1

We first reveal entanglement phase transitions in the NHA AH1 by investigating its steady-state EE  $S(L, l)$ , with  $L$  and  $l$  being the length of lattice and the size of its subsystem A. The system is prepared at  $t = 0$  in the initial state  $|\Psi_0\rangle$  [Eq. (11)] and then evolved according to Eq. (10), with the  $\hat{H}$  given by Eq. (1). The EE  $S(t)$  at a later time  $t$  [Eq. (13)] is obtained from the spectrum of correlation matrix  $C(t)$  [Eq. (12)] restricted to the subsystem A. Focusing on a long-time evolution of duration  $T$ , we obtain the steady-state EE  $S(L, l)$  by averaging  $S(t)$  over a suitable time window  $t \in [T', T]$  with  $1 \ll T' < T$ . The scaling property of  $S(L, l)$  can then be analyzed by considering different choices of  $L$  and  $l$ .

In Fig. 2, we present the steady-state EE versus the system size  $L$  and the subsystem size  $l$  for typical sets of system parameters. In Figs. 2(a) and 2(c), we consider a equal bipartition of the system ( $l = \lfloor L/2 \rfloor$ ). For  $|V| > |J|$ , we find that the  $S(L, L/2)$  almost does not change with  $L$ , which implies that the PT-broken localized phase of the NHA AH1 is area-law entangled. This is expected, as in this case the point dissipation gap on the complex energy plane [see Eq. (3)] and the spatial localization of all eigenstates both tend to hinder the spreading of quantum entanglement across the system. For  $|V| < |J|$ , we instead observe that up to leading order, the EE is proportional to the system size  $L$ , i.e.,

$S(L, L/2) \propto gL$  with the gradient  $g \approx 0.1 \sim 0.2$ . Therefore, in the PT-invariant extended phase of NHA AH1, the steady-state EE tends to satisfy a volume-law. Such a linear scaling is triggered by the quantum information spreading due to delocalized bulk states with real energies in the system. The gradient  $g$  of the volume-law scaling decreases gradually but remains finite till the critical point of PT and localization transitions at  $|J| = |V|$ .

In Figs. 2(b) and 2(d), we consider a fixed system size  $L$  and obtain the curve  $S(L, l)$  vs the size  $l$  of subsystem A for  $l \in (0, L)$ . The results show that for  $|V| > |J|$ , the  $S(L, l)$  is almost independent of  $l$  up to slight fluctuations, which is an expected situation for an area-law entangled phase. For  $|V| < |J|$ , the  $S(L, l)$  as a function of  $l$  can be numerically fitted as  $S(L, l) \simeq A \sin(\pi l/L) + B \ln[\sin(\pi l/L)] + C$ , where  $A$ ,  $B$  and  $C$  are some fitting coefficients. This is typical for a volume-law entangled phase. Putting together, we conclude that the steady-state EE of NHA AH1 indeed follows qualitatively different scaling laws with respect to the (sub)system size in different parameter regions, which implies the presence of entanglement phase transitions in the system.

To further decipher the entanglement transitions in NHA AH1, we present its steady-state EE  $S(L, L/2)$  versus  $V$  and  $J$  for different system sizes  $L$  in Figs. 3(a) and 3(c). Two distinct regions can be clearly figured out. In the region with  $|J| < |V|$ , the EE shows an  $L$ -independence. Whereas for  $|J| > |V|$ , the EE in-

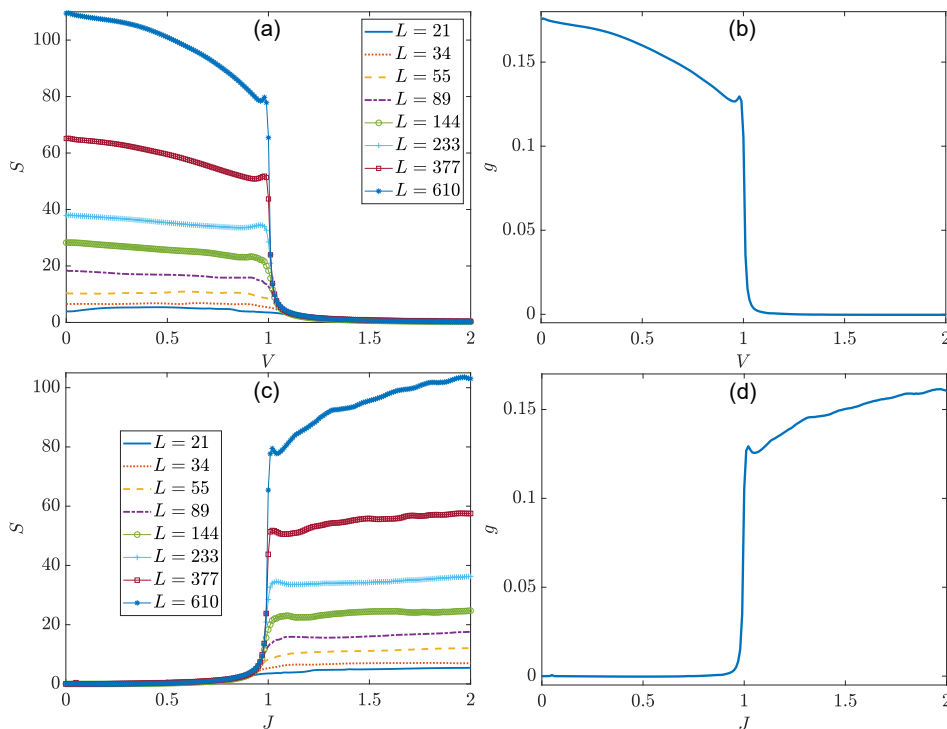


FIG. 3. Bipartite EE of the steady state at half-filling [in (a), (c)] and the related gradient  $g$  in the scaling law of steady-state EE [in (b) and (d)] for the NHAH1. Other system parameters are set as  $J = 1$  for (a), (b) and  $V = 1$  for (c), (d). The time span of the entire evolution is  $T = 1000$  [113]. The values of  $g$  are obtained from the linear fitting  $S(L, L/2) \sim gL + s_0$  of EE versus the lattice size  $L$  at given system parameters.

increases monotonically with  $L$ . A marked change is observed at  $|J| = |V|$  in the  $L$ -dependence of  $S(L, L/2)$ , which implies a transition in the scaling law of EE. In Figs. 3(b) and 3(d), we obtain the gradient  $g$  by fitting the steady-state EE  $S(L, L/2)$  with the function  $gL + s_0$  at different values of  $J$  and  $V$ . The results show that  $g \simeq 0$  [ $S(L, L/2) \sim s_0 \sim L^0$ ] for  $|J| < |V|$  and  $g > 0$  [ $S(L, L/2) \propto L$ ] for  $|J| > |V|$ , which are expected behaviors for area-law entangled and volume-law entangled phases, respectively. There is then a discontinuous change of  $g$  at  $|J| = |V|$ , which signifies an entanglement phase transition in the NHAH1.

The physics behind the different scaling laws of EE is as follows. For our NHAH1, initial excitations could propagate and spread uniformly across the whole lattice with the increase of time for  $|V| < |J|$ , i.e., in the PT-invariant extended phase, and the entanglement is building up throughout the system before reaching a steady state. When the steady-state is reached, an extensive entanglement is retained across any spatial cuts in the lattice. The resulting bipartite EE then follows a volume-law ( $gL$ ) vs the system size. For  $|V| > |J|$ , all the eigenstates are localized, and any initial excitations could not propagate and spread in the system after an initial transient time window. Moreover, the onsite gain and loss are strong enough when  $|V| > |J|$  so as to disentangle degrees of freedom at different spatial locations. Therefore, any extensive entanglement could not be established across

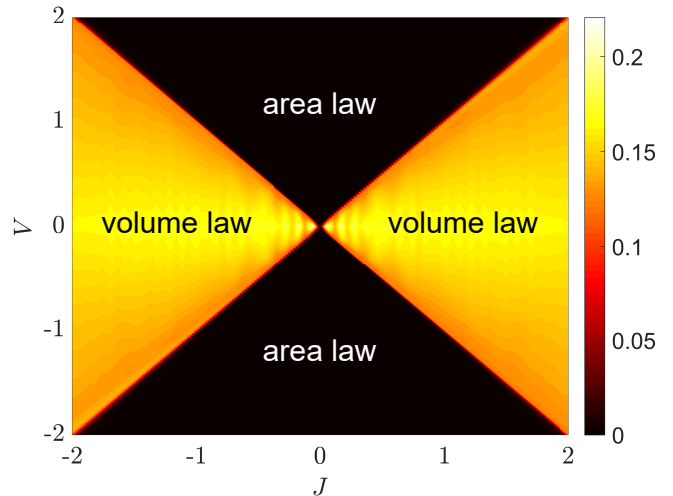


FIG. 4. Entanglement phase diagram of the NHAH1. Different colors correspond to different values of the gradient  $g$  extracted from the linear fitting  $S(L, L/2) \sim gL + s_0$  of steady-state EE versus the system size  $L$ .

the system due to the collaboration between strong disorder and strong gain/loss (which may also be viewed as strong measurement backactions [63]). The result is an area-law scaling of steady-state EE versus the system size in the PT-broken localized phase of our system.

NHAAH1	$ V  <  J $	$ V  =  J $	$ V  >  J $
Energy spectrum	real	PT transition	complex
Eigenstates	extended	localization transition	localized
Steady-state EE	volume-law	entanglement transition	area-law

TABLE I. Summary of main results for the quasicrystal NHAAH1. The real-spectrum (PT-invariant), extended phase is volume-law entangled. The complex-spectrum (PT-broken), localized phase is area-law entangled. The PT, localization and entanglement phase transitions happen all together at  $|V| = |J|$  [see also Figs. 1(a), 1(b) and 4].

Collecting together the scaling properties of steady-state EE with respect to the lattice size  $L$  for a half-filled and bipartite system, we arrive at the entanglement phase diagram of NHAAH1 under the PBC in Fig. 4. A summary of the key features of NHAAH1 is given in Table I. We find that there are indeed two phases with different entanglement nature, which are separated by an entanglement transition at  $|J| = |V|$ . In the PT-broken localized phase ( $|J| < |V|$ ), the system is found to be area-law entangled [ $S(L, L/2) \sim L^0$ ]. The spectrum is complex with a point dissipation gap at  $E = 0$  on the complex energy plane [see Eq. (3)] and all the eigenstates are localized, both compelling the termination of entanglement spreading in this case. In the PT-invariant extended phase ( $|J| > |V|$ ), the system is instead volume-law entangled [ $S(L, L/2) \propto L$  up to the leading order]. Since the system possesses a real spectrum [Eq. (3)] and all its eigenstates are extended in this case, the quantum information is forced to spread and a volume-law entangled phase results. Such a volume-law to area-law entanglement phase transition was identified before in clean non-Hermitian systems due to different physical mechanisms [62, 63]. In the next subsection, we will demonstrate that an even more exotic type of entanglement phase transition could emerge in NHQCs due to the interplay between disorder and nonreciprocity.

## B. NHAAH2

We now explore the entanglement phase transitions in the NHAAH2 [Eq. (4)] by inspecting the steady-state EE  $S(L, l)$  of a subsystem A, where  $L$  is the length of lattice and  $l$  is the subsystem size. The initial state of the system is still at half-filling and described by the wavefunction  $|\Psi_0\rangle$  in Eq. (11). Evolving  $|\Psi_0\rangle$  over a long time duration  $T$  from  $t = 0$ , we obtain the EE  $S(t)$  at each  $t \in [0, T]$  according to Eqs. (10)–(13). The steady-state  $S(L, l)$  is then extracted by averaging  $S(t)$  over a time duration  $t \in [T', T]$  for an appropriately chosen  $1 \ll T' < T$ . We could then analyze the scaling behavior of  $S(L, l)$  with respect to the system size  $L$  or the subsystem size  $l$  at any give sets of system parameters  $(J, V)$ .

Similar to the NHAAH1, we first consider a bipartite system with  $l = \lfloor L/2 \rfloor$  for the NHAAH2. The  $L$ -dependence of  $S(L, L/2)$  for some typical cases are then obtained and shown in Fig. 5. We find that the EE almost does not change with  $L$  for  $|V| > |J|$ , which suggests that

the PT-invariant localized phase of the NHAAH2 is area-law entangled. At  $J = V = 1$ , we find that up to the leading order  $S(L, L/2) \sim gL$ , with the gradient  $g \approx 0.1$ . The same scaling law is found for other values of  $J = V \neq 0$ , which indicates that the NHAAH2 is volume-law entangled along the critical lines  $J = \pm V$  of the PT-breaking and localization transitions. Interestingly, we find that up to the leading order  $S(L, L/2) \sim g \ln L$  for the cases with  $|V| < |J|$ , where the coefficient  $g \approx 0.34$ . Therefore, the PT-broken extended phase of the NHAAH2 tends out to be log-law entangled. Such an abnormal entanglement behavior is clearly distinct from typical scaling laws of steady-state EE found in other non-Hermitian systems due to non-Hermitian skin effects or line dissipation gaps [62, 63]. The qualitative change in the scaling law of steady-state EE from  $|V| < |J|$  to  $|V| > |J|$  further suggests a log-law to area-law entanglement transition, which is mediated by a critical volume-law entangled phase along  $|V| = |J|$ .

To further decode the entanglement transitions in the NHAAH2, we consider the EE  $S(L, l)$  versus the subsystem size  $l$  for a fixed  $L$ , with typical results at different system parameters shown in Fig. 6. For the cases with  $|V| > |J|$ , we find that the  $S(L, l)$  is almost independent of  $l$  up to small oscillations, which is typical for an area-law entangled phase. At  $J = V = 1$ , the  $S(L, l)$  has the shape of the function  $A \sin(\pi l/L) + B \ln[\sin(\pi l/L)] + C$  with a small offset at  $l = L/2$ . Interestingly, our numerics suggest the following generic form of EE for  $|V| < |J|$ , i.e.,

$$S(L, l) \simeq \frac{c}{6} \ln[\sin(\pi l/L)] + S_0, \quad (14)$$

where  $S_0$  is a non-universal constant. Away from the transition point  $|V| = |J|$ , the value of  $c$  is found to be 2 with the numerical error of order  $10^{-3}$ . Referring to the typical form of  $S(L, l)$  for a one-dimensional (1D) quantum critical system [62], Eq. (14) implies a central charge  $c = 2$  for the PT-broken extended phase of the NHAAH2. The physical origin of this central charge might be understood from the fact that at half filling, there are two Fermi points with  $E = 0$  at  $k = \pm\pi/2$  on the Fermi surface [see Eq. (7)]. Each of them makes a contribution one to the central charge  $c$ . Compared with the forms of  $S(L, l)$  in Figs. 2(b) and 2(d) for the NHAAH1, we further realize that the NHAAH2 should indeed possess a phase with unique entanglement nature as described by the scaling relation (14).

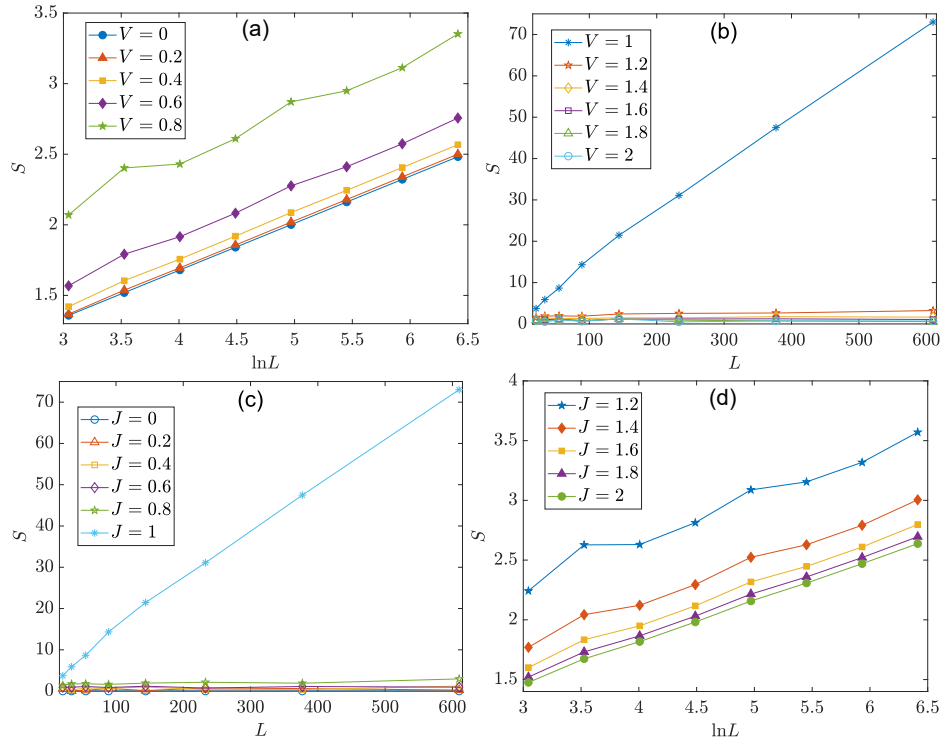


FIG. 5. Steady-state EE of the NHAH2 versus the system size  $L$  at half-filling and under equal bipartition. Other system parameters are set as  $J = 1$  for (a), (b) and  $V = 1$  for (c), (d). The time span of the entire dynamics is  $T = 1000$  [113].

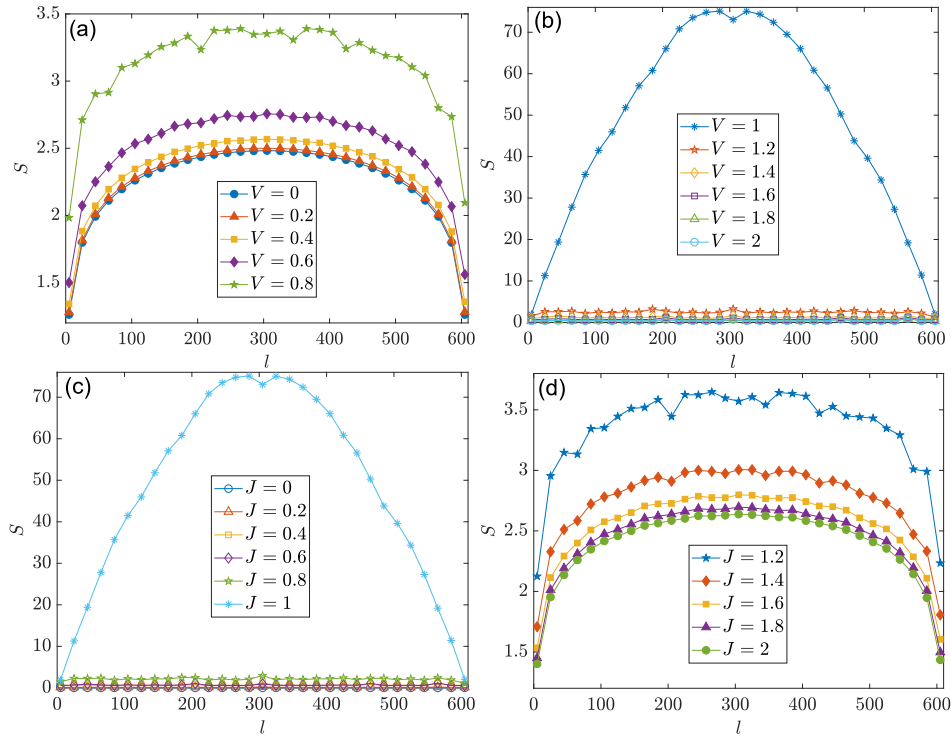


FIG. 6. Steady-state EE of the NHAH2 vs the subsystem size  $l$  at half-filling and under a fixed length of lattice  $L = 610$ . Other system parameters are  $J = 1$  for (a), (b) and  $V = 1$  for (c), (d). The time span of the entire dynamics is  $T = 1000$  [113].



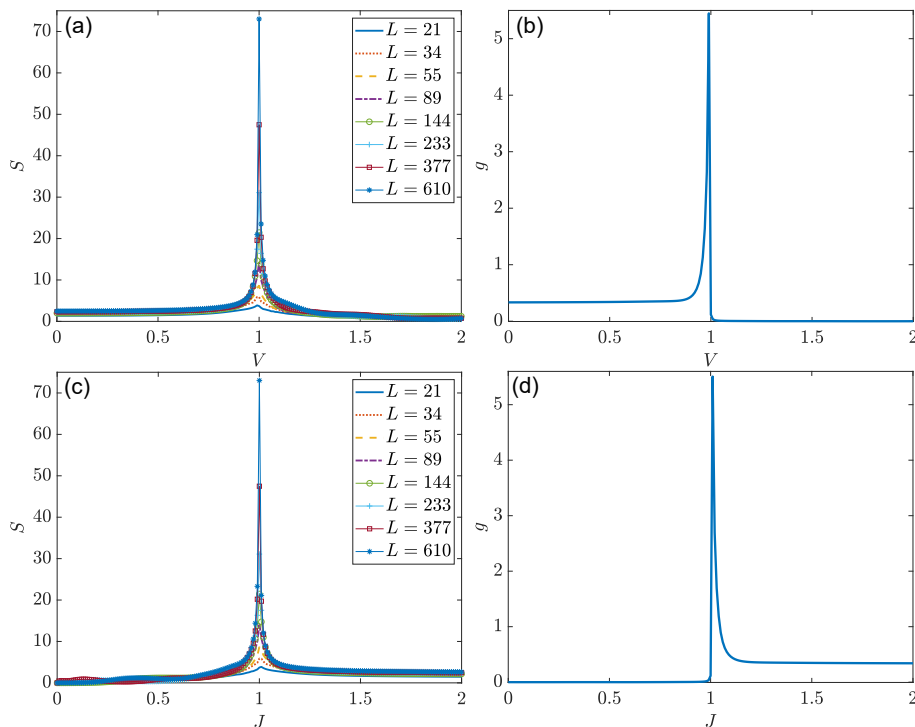


FIG. 7. Bipartite EE of the steady state at half-filling [in (a), (c)] and the related gradient  $g$  in the scaling law of steady-state EE [in (b) and (d)] for the NHAH2. Other system parameters are set as  $J = 1$  for (a), (b) and  $V = 1$  for (c), (d). The time span of the entire evolution is  $T = 1000$  [113]. The values of  $g$  are obtained from the linear fitting  $S \sim gL + s_0$  ( $S \sim g \ln L + s_0$ ) of EE versus the system size  $L$  for  $J \leq V$  ( $J > V$ ) in (b) and (d).

Combining the information obtained from the scaling properties of EE with respect to the system size, we are now ready to reveal the entanglement phase transitions in the NHAH2. In Figs. 7(a) and 7(c), we present the steady-state EE versus  $V$  and  $J$  for different system sizes. A clear peak can be identified at  $J = V$ , whose height increases monotonically with the increase of the lattice size  $L$ . The presence of such a sharp peak in  $S(L, L/2)$  clearly hints at the occurrence of an entanglement transition at  $J = V$ . In Figs. 7(b) and 7(d), we use the relations  $S \sim gL + s_0$  and  $S \sim g \ln L + s_0$  to fit the data at different  $L$  for  $|J| \leq |V|$  and  $|J| > |V|$ , respectively. The results suggest that the scaling form of EE could undergo a discontinuous change from a log-law ( $|V| < |J|$ ) with a finite  $g$  in  $S \sim g \ln L + s_0$  to an area-law with  $g \simeq 0$  in the linear fitting  $S \sim gL + s_0$  ( $|V| > |J|$ ). There is thus an entanglement phase transition at  $|V| = |J|$  accompanying the PT and localization transitions in the NHAH2.

To have a more balanced comparison between the scaling laws in different parameter regions, we could assume a fitting function  $S(L, L/2) \sim g \ln L + g' L + s_0$ . Our numerical calculations then suggest that  $g \simeq 0.34$  and  $g' \simeq 0$  in the region  $|V| < |J|$ , while  $g \simeq 0$  and  $g' \simeq 0$  in the region  $|V| > |J|$ . These two regions thus correspond to log-law and area-law entangled phases. Right at  $|V| = |J|$ , we find  $g \simeq 2.4$  and  $g' \simeq 0.1$ , and the volume-law scaling dominates with the increase of  $L$ .

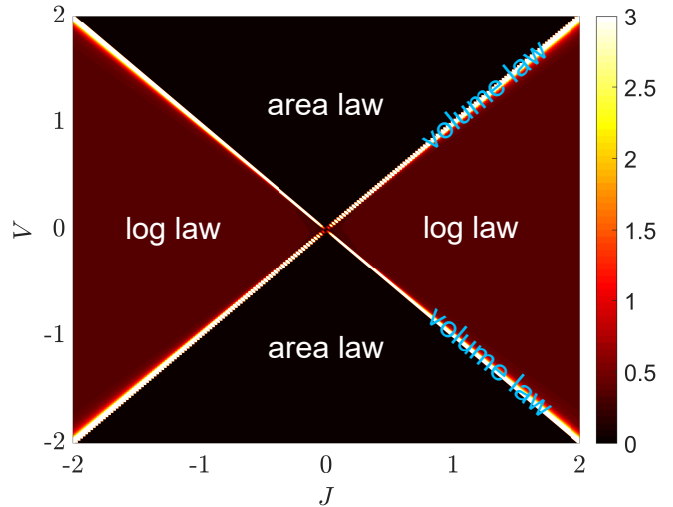


FIG. 8. Entanglement phase diagram of the NHAH2. Different colors correspond to different values of the gradient  $g$  extracted from the fitting  $S \sim gL + s_0$  ( $S \sim g \ln L + s_0$ ) of steady-state EE versus the system size  $L$  for  $|V| \geq |J|$  ( $|V| < |J|$ ).

Finally, we establish the entanglement phase diagram of the NHAH2 by extracting the scaling laws of steady-state EE versus the system size  $L$  for a half-filled and bipartite lattice under the PBC, as shown in Fig. 8.



NHAAH2	$ V  <  J $	$ V  =  J $	$ V  >  J $
Energy spectrum	complex	PT transition	real
Eigenstates	extended	localization transition	localized
Steady-state EE	log-law	volume-law	area-law

TABLE II. Summary of main results for the quasicrystal NHAAH2 4. The complex-spectrum (PT-broken), extended phase is log-law entangled. The real-spectrum (PT-invariant), localized phase is area-law entangled. The PT, localization and entanglement transitions happen all together at  $|V| = |J|$ , where the steady-state EE follows the volume-law as in NHAAH1 [see also Figs. 1(c), 1(d) and 8].

We observe that the EE indeed satisfies an area law [ $S(L, L/2) \sim L^0$ ] in the PT-invariant localized phase ( $|J| < |V|$ ), and fulfills an anomalous log-law scaling [ $S(L, L/2) \propto \ln L$ ] in the PT-broken extended phase ( $|J| > |V|$ ). Along the phase boundary ( $|J| = |V|$ ), the EE shows a volume-law critical scaling behavior [ $S(L, L/2) \propto L$ ], which is similar to the NHAAH1. Besides that, the entangled phases and entanglement transitions in the NHAAH2 are rather different from those appeared in NHAAH1. A summary of the key features of NHAAH2 is given in Table II.

A possible reason behind these differences is as follows. In the PT-broken extended phase of NHAAH2 ( $|J| > |V|$ ), the asymmetric hopping overcomes the block of quasiperiodic disorder and allows the spreading of quantum information across the system, yielding the tendency of forming an extensively entangled phase. However, the spectrum of the system in the PT-broken phase possesses a point gap on the complex energy plane at  $E = 0$  [see Eq. (7)]. The presence of such a dissipation gap tends to suppress the quantum information spreading and prefers an area-law scaling for the steady-state EE. The competition between these two opposite tendencies ends up with a compromise, as reflected by the log-law entangled phase in Fig. 8. In the PT-invariant localized phase of NHAAH2 ( $|J| < |V|$ ), the disorder is strong enough to prevent the information spreading and stabilizes the system in an area-law entangled phase, even though the energy spectrum is fully real [see Eq. (7)]. The very different entanglement dynamics in our mutually dual NHQC models could thus be understood. The clear differences between the entanglement transitions discovered here and some typical situations encountered in previous studies [59, 62, 63] further highlight the interesting role played by disorder in non-Hermitian systems from a quantum information perspective.

#### IV. CONCLUSION AND DISCUSSION

In this work, we revealed entanglement phase transitions in representative 1D NHQCs. In a system with onsite gain and loss, a volume-law to area-law transition in the steady-state EE was found to go hand-in-hand with PT-breaking and localization transitions induced by non-Hermitian quasiperiodic potentials. In a system with nonreciprocal hopping, the steady-state EE

instead showcased an area-law to log-law entanglement transition with the increase of the hopping asymmetry, which was mediated by a critical entangling phase whose EE followed a volume-law scaling versus the system size. This transition also went hand-in-hand with PT-breaking and delocalization transitions due to the interplay between hopping nonreciprocity and spatial quasiperiodicity. Even though the two considered models can be viewed as dual to each other, they exhibited rather different entanglement dynamics except at critical points, which were demonstrated in detail by our numerical analysis of their EE scaling laws and entanglement phase diagrams. Our findings thus unveiled the richness of entanglement phases and transitions in non-Hermitian disordered systems, which may find applications in quantum error correction and quantum information storage against decoherence.

As we focused on phases and entanglement dynamics of the bulk of NHQCs, the PBC was taken throughout our calculations. A consistent framework regarding PT transitions, localization transitions and entanglement transitions were then established for our “minimal” NHQC models under PBC, and rich patterns of entanglement transitions were identified. Under open boundary conditions, there could be edge states in our models, whose numbers are much smaller than the bulk states. The NHAAH2 would further show non-Hermitian skin effects. A complete treatment of their interplay with entanglement transitions under different boundary conditions would thus be an interesting direction of future research.

In Figs. 2 and 6, some asymmetries are observed in  $S(L, l)$  vs  $l$  with  $L = 610$  when the system parameters are approaching the phase boundaries ( $|J| = |V|$  for both models). One possible origin of these asymmetries is the instability of numerical calculations around the critical points of phase transitions. Another possible source is that at the critical point of localization transition, the quasicrystal may show multifractal properties, and correction terms other than the volume-law or log-law may appear in the subsystem-size scaling of EE, even though the volume-law or log-law behavior still dominates. Our numerical resolutions could not figure out all these correction terms at present. An in-depth analysis about the critical properties and universality classes of entanglement phase transitions in NHQCs is thus necessary in future studies.

Our model NHAAH1 [Eq. (1)] possesses onsite gain and loss. In theory, it might be viewed as the no-click limit of a monitored AAH model. The gain and loss in the system may then be understood as imaginary chemical potentials induced by measurement backactions [52, 63]. In practice, cold atom systems [114–118] could be considered as candidates to realize our models. For fermions, one may introduce state-selective atom loss by using a near-resonant laser beam to kick atoms out of a trap [117]. The negative imaginary part of onsite potential in our NHAAH1 then describes the loss rate. Realizing atom gain for fermions is more challenging. One may instead add a uniform background loss  $-i\gamma \sum_n \hat{c}_n^\dagger \hat{c}_n$  with  $\gamma > 0$  to our NHAAH1 and let  $\gamma > |V|$ . In this case, there is no gain in the system, yet the Hamiltonian loses its PT-symmetry in strict sense. Nevertheless, we can still find the spectrum transformation from a line segment (with  $|V| < |J|$ ) to an ellipse (with  $|V| > |J|$ ), which is now centered at  $(0, -i\gamma)$  on the complex plane. The particle dynamics and EE dynamics are not affected by such a uniform background loss according to Eqs. (10)–(13). Additionally, the unidirectional hopping of our NHAAH2 might be realized by implementing asymmetric quantum walks of cold atoms in momentum space [118], which is not sensitive to particle statistics. Putting together, our non-Hermitian fermionic models should be physically realizable in near-term experiments.

Although our results are obtained by investigating two “minimal” NHQC models, we expect to find simi-

lar patterns of entanglement phase transitions in other 1D NHQCs with simultaneous PT and localization transitions, such as those considered in Refs. [70, 71, 108]. In more general situations, the extended and localized phases of an NHQC could be separated by a critical phase, in which extended and localized eigenstates coexist and are separated by mobility edges. The entanglement transition in NHQCs with mobility edges thus constitutes another interesting direction of future research. Besides, much less is known regarding entanglement transitions in non-Hermitian disordered systems beyond one spatial dimension, with uncorrelated disorder [119–121] and with many-body interactions [122, 123]. Concrete experimental signatures of entanglement phase transitions in non-Hermitian systems also deserve more thorough considerations.

*Note added:* Before the submission of this work, we realized a new preprint [124], which also explored entanglement phase transitions in NHQCs with a focus on the interplay between disorder and non-Hermitian skin effects.

## ACKNOWLEDGMENTS

This work is supported by the National Natural Science Foundation of China (Grant Nos. 12275260 and 11905211), the Fundamental Research Funds for the Central Universities (Grant No. 202364008), and the Young Talents Project of Ocean University of China.

- 
- [1] Y. Li, X. Chen, and M. P. A. Fisher, Quantum Zeno Effect and the Many-Body Entanglement Transition, *Phys. Rev. B* **98**, 205136 (2018).
  - [2] B. Skinner, J. Ruhman, and A. Nahum, Measurement-Induced Phase Transitions in the Dynamics of Entanglement, *Phys. Rev. X* **9**, 031009 (2019).
  - [3] A. Chan, R. M. Nandkishore, M. Pretko, and G. Smith, Unitary-Projective Entanglement Dynamics, *Phys. Rev. B* **99**, 224307 (2019).
  - [4] Y. Li, X. Chen, and M. P. A. Fisher, Measurement-Driven Entanglement Transition in Hybrid Quantum Circuits, *Phys. Rev. B* **100**, 134306 (2019).
  - [5] X. Cao, A. Tilloy, and A. D. Luca, Entanglement in a Fermion Chain under Continuous Monitoring, *SciPost Phys.* **7**, 024 (2019).
  - [6] M. Szyniszewski, A. Romito and H. Schomerus, Entanglement transition from variable-strength weak measurements, *Phys. Rev. B* **100**, 064204 (2019).
  - [7] R. Vasseur, A. C. Potter, Y.-Z. You and A. W. W. Ludwig, Entanglement transitions from holographic random tensor networks, *Phys. Rev. B* **100**, 134203 (2019).
  - [8] S. Choi, Y. Bao, X.-L. Qi, and E. Altman, Quantum Error Correction in Scrambling Dynamics and Measurement-Induced Phase Transition, *Phys. Rev. Lett.* **125**, 030505 (2020).
  - [9] Y. Bao, S. Choi, and E. Altman, Theory of the Phase Transition in Random Unitary Circuits with Measurements, *Phys. Rev. B* **101**, 104301 (2020).
  - [10] C.-M. Jian, Y.-Z. You, R. Vasseur, and A. W. W. Ludwig, Measurement-Induced Criticality in Random Quantum Circuits, *Phys. Rev. B* **101**, 104302 (2020).
  - [11] Y. Fuji and Y. Ashida, Measurement-Induced Quantum Criticality under Continuous Monitoring, *Phys. Rev. B* **102**, 054302 (2020).
  - [12] M. J. Gullans and D. A. Huse, Dynamical Purification Phase Transition Induced by Quantum Measurements, *Phys. Rev. X* **10**, 041020 (2020).
  - [13] M. Szyniszewski, A. Romito and H. Schomerus, Universality of entanglement transitions from stroboscopic to continuous measurements, *Phys. Rev. Lett.* **125**, 210602 (2020).
  - [14] O. Lunt and A. Pal, Measurement-induced entanglement transitions in many-body localized systems, *Phys. Rev. Res.* **2**, 043072 (2020).
  - [15] M. J. Gullans and D. A. Huse, Scalable probes of measurement-induced criticality, *Phys. Rev. Lett.* **125**, 070606 (2020).
  - [16] A. Zabalo, M. J. Gullans, J. H. Wilson, S. Gopalakrishnan, D. A. Huse and J. H. Pixley, Critical properties of the measurement-induced transition in random quantum circuits, *Phys. Rev. B* **101**, 060301 (2020).
  - [17] X. Turkeshi, R. Fazio and M. Dalmonte, Measurement-induced criticality in (2+1)-dimensional hybrid quantum circuits, *Phys. Rev. B* **102**, 014315 (2020).
  - [18] X. Chen, Y. Li, M. P. A. Fisher, and A. Lucas, Emergent conformal symmetry in nonunitary random dynamics of

- free fermions, *Phys. Rev. Res.* **2**, 033017 (2020).
- [19] A. Nahum and B. Skinner, Entanglement and dynamics of diffusion-annihilation processes with Majorana defects, *Phys. Rev. Res.* **2**, 023288 (2020).
- [20] Q. Tang and W. Zhu, Measurement-induced phase transition: A case study in the nonintegrable model by density-matrix renormalization group calculations, *Phys. Rev. Res.* **2**, 013022 (2020).
- [21] S. Goto and I. Danshita, Measurement-induced transitions of the entanglement scaling law in ultracold gases with controllable dissipation, *Phys. Rev. A* **102**, 033316 (2020).
- [22] J. Iaconis, A. Lucas, and X. Chen, Measurement-induced phase transitions in quantum automaton circuits, *Phys. Rev. B* **102**, 224311 (2020).
- [23] J. Lopez-Piqueres, B. Ware, and R. Vasseur, Mean-field entanglement transitions in random tree tensor networks, *Phys. Rev. B* **102**, 064202 (2020).
- [24] B. Bertini and L. Piroli, Scrambling in random unitary circuits: Exact results, *Phys. Rev. B* **102**, 064305 (2020).
- [25] A. Lavasani, Y. Alavirad, and M. Barkeshli, Measurement-Induced Topological Entanglement Transitions in Symmetric Random Quantum Circuits, *Nat. Phys.* **17**, 342 (2021).
- [26] S. Sang and T. H. Hsieh, Measurement-Protected Quantum Phases, *Phys. Rev. Res.* **3**, 023200 (2021).
- [27] M. Ippoliti, M. J. Gullans, S. Gopalakrishnan, D. A. Huse, and V. Khemani, Entanglement Phase Transitions in Measurement-Only Dynamics, *Phys. Rev. X* **11**, 011030 (2021).
- [28] O. Alberton, M. Buchhold, and S. Diehl, Entanglement Transition in a Monitored Free-Fermion Chain: From Extended Criticality to Area Law, *Phys. Rev. Lett.* **126**, 170602 (2021).
- [29] M. Ippoliti and V. Khemani, Postselection-Free Entanglement Dynamics via Spacetime Duality, *Phys. Rev. Lett.* **126**, 060501 (2021).
- [30] T.-C. Lu and T. Grover, Spacetime Duality between Localization Transitions and Measurement-Induced Transitions, *PRX Quantum* **2**, 040319 (2021).
- [31] A. Biella and M. Schiró, Many-body quantum Zeno effect and measurement-induced subradiance transition, *Quantum* **5**, 528 (2021).
- [32] X. Turkeshi, Measurement-induced criticality as a data-structure transition, *Phys. Rev. B* **106**, 144313 (2021).
- [33] J. Iaconis and X. Chen, Multifractality in nonunitary random dynamics, *Phys. Rev. B* **104**, 214307 (2021).
- [34] Y. Li, X. Chen, A. W. W. Ludwig and M. P. A. Fisher, Conformal invariance and quantum nonlocality in critical hybrid circuits, *Phys. Rev. B* **104**, 104305 (2021).
- [35] O. Lunt, M. Sznyszewski and A. Pal, Measurement-induced criticality and entanglement clusters: A study of one-dimensional and two-dimensional Clifford circuits, *Phys. Rev. B* **104**, 155111 (2021).
- [36] S.-K. Jian, C. Liu, X. Chen, B. Swingle, and P. Zhang, Measurement-Induced Phase Transition in the Monitored Sachdev-Ye-Kitaev Model, *Phys. Rev. Lett.* **127**, 140601 (2021).
- [37] A. Nahum, S. Roy, B. Skinner, and J. Ruhman, Measurement and Entanglement Phase Transitions in All-To-All Quantum Circuits, on Quantum Trees, and in Landau-Ginsburg Theory, *PRX Quantum* **2**, 010352 (2021).
- [38] M. Buchhold, Y. Minoguchi, A. Altland, and S. Diehl, Effective Theory for the Measurement-Induced Phase Transition of Dirac Fermions, *Phys. Rev. X* **11**, 041004 (2021).
- [39] S. Sang, Y. Li, T. Zhou, X. Chen, T. H. Hsieh, and M. P. A. Fisher, Entanglement Negativity at Measurement-Induced Criticality, *PRX Quantum* **2**, 030313 (2021).
- [40] T. Botzung, S. Diehl, and M. Müller, Engineered dissipation induced entanglement transition in quantum spin chains: From logarithmic growth to area law, *Phys. Rev. B* **104**, 184422 (2021).
- [41] M. Ippoliti, T. Rakovszky, and V. Khemani, Fractal, Logarithmic, and Volume-Law Entangled Nonthermal Steady States via Spacetime Duality, *Phys. Rev. X* **12**, 011045 (2022).
- [42] T. Boorman, M. Sznyszewski, H. Schomerus and A. Romito, Diagnostics of entanglement dynamics in noisy and disordered spin chains via the measurement-induced steady-state entanglement transition, *Phys. Rev. B* **105**, 144202 (2022).
- [43] F. Barratt, U. Agrawal, A. C. Potter, S. Gopalakrishnan and R. Vasseur, Transitions in the learnability of global charges from local measurements, *Phys. Rev. Lett.* **129**, 200602 (2022).
- [44] F. Barratt, U. Agrawal, S. Gopalakrishnan, D. A. Huse, R. Vasseur and A. C. Potter, Field theory of charge sharpening in symmetric monitored quantum circuits, *Phys. Rev. Lett.* **129**, 120604 (2022).
- [45] A. Zabalo, M. J. Gullans, J. H. Wilson, R. Vasseur, A. W. W. Ludwig, S. Gopalakrishnan, David A. Huse, and J. H. Pixley, Operator scaling dimensions and multifractality at measurement-induced transitions, *Phys. Rev. Lett.* **128**, 050602 (2022).
- [46] P. Sierant, G. Chiriacó, F. M. Surace, S. Sharma, X. Turkeshi, M. Dalmonte, R. Fazio, and G. Pagano, Dissipative Floquet dynamics: From steady state to measurement induced criticality in trapped-ion chains, *Quantum* **6**, 638 (2022).
- [47] M. Block, Y. Bao, S. Choi, E. Altman and N. Y. Yao, Measurement-induced transition in long-range interacting quantum circuits, *Phys. Rev. Lett.* **128**, 010604 (2022).
- [48] U. Agrawal, A. Zabalo, K. Chen, J. H. Wilson, A. C. Potter, J. H. Pixley, S. Gopalakrishnan and R. Vasseur, Entanglement and charge-sharpening transitions in  $U(1)$  symmetric monitored quantum circuits, *Phys. Rev. X* **12**, 041002 (2022).
- [49] S. Sharma, X. Turkeshi, R. Fazio and M. Dalmonte, Measurement-induced criticality in extended and long-range unitary circuits, *SciPost Phys. Core* **5**, 023 (2022).
- [50] P. Sierant and X. Turkeshi, Universal behavior beyond multifractality of wave functions at measurement-induced phase transitions, *Phys. Rev. Lett.* **128**, 130605 (2022).
- [51] Z.-C. Yang, Y. Li, M. P. A. Fisher, and X. Chen, Entanglement phase transitions in random stabilizer tensor networks, *Phys. Rev. B* **105**, 104306 (2022).
- [52] X. Turkeshi and M. Schiró, Entanglement and correlation spreading in non-Hermitian spin chains, *Phys. Rev. B* **107**, L020403 (2023).
- [53] C. Noel, P. Niroula, D. Zhu, A. Risinger, L. Egan, D. Biswas, M. Cetina, A. V. Gorshkov, M. J. Gullans, D. A. Huse, and C. Monroe, Measurement-induced quantum phases realized in a trapped-ion quantum computer,

- Nat. Phys. **18**, 760 (2022).
- [54] J. M. Koh, S.-N. Sun, M. Motta, and A. J. Minnich, Measurement-induced entanglement phase transition on a superconducting quantum processor with mid-circuit readout, Nat. Phys. **19**, 1314-1319 (2023).
- [55] Google Quantum AI and Collaborators, Measurement-induced entanglement and teleportation on a noisy quantum processor, Nature **622**, 481-486 (2023).
- [56] A. C. Potter and R. Vasseur, Entanglement dynamics in hybrid quantum circuits, in Quantum science and technology, Springer International Publishing, Cham, Switzerland, ISBN 9783031039973 (2022).
- [57] M. P. A. Fisher, V. Khemani, A. Nahum, and S. Vijay, Random Quantum Circuits, Annu. Rev. Condens. Matter Phys. **14**, 335 (2023).
- [58] B. Skinner, Introduction to random unitary circuits and the measurement-induced entanglement phase transition, arXiv:2307.02986.
- [59] Á. Bácsi and B. Dóra, Dynamics of entanglement after exceptional quantum quench, Phys. Rev. B **103**, 085137 (2021).
- [60] S. Gopalakrishnan and M. J. Gullans, Entanglement and Purification Transitions in Non-Hermitian Quantum Mechanics, Phys. Rev. Lett. **126**, 170503 (2021).
- [61] X. Turkeshi, M. Dalmonte, R. Fazio, and M. Schirò, Entanglement transitions from stochastic resetting of non-Hermitian quasiparticles, Phys. Rev. B **105**, L241114 (2022).
- [62] K. Kawabata, T. Numasawa, and S. Ryu, Entanglement Phase Transition Induced by the Non-Hermitian Skin Effect, Phys. Rev. X **13**, 021007 (2023).
- [63] Y. L. Gal, X. Turkeshi and M. Schirò, Volume-to-area law entanglement transition in a non-Hermitian free fermionic chain, SciPost Phys. **14**, 138 (2023).
- [64] E. Granet, C. Zhang, and H. Dreyer, Volume-Law to Area-Law Entanglement Transition in a Nonunitary Periodic Gaussian Circuit, Phys. Rev. Lett. **130**, 230401 (2023).
- [65] L. Zhou, Entanglement phase transitions in non-Hermitian Floquet systems, arXiv:2310.11351.
- [66] T. Qian, Y. Gu, and L. Zhou, Correlation-induced phase transitions and mobility edges in an interacting non-Hermitian quasicrystal, arXiv:2310.01275.
- [67] P. Sarnak, Spectral behavior of quasi periodic potentials, Commun. Math. Phys. **84**, 377 (1982).
- [68] A. Jazaeri and I. I. Satija, Localization transition in incommensurate non-Hermitian systems, Phys. Rev. E **63**, 036222 (2001).
- [69] Q. Zeng, S. Chen, and R. Lü, Anderson localization in the non-Hermitian Aubry-André-Harper model with physical gain and loss, Phys. Rev. A **95**, 062118 (2017).
- [70] H. Jiang, L. Lang, C. Yang, S. Zhu, and S. Chen, Interplay of non-Hermitian skin effects and Anderson localization in nonreciprocal quasiperiodic lattices, Phys. Rev. B **100**, 054301 (2019).
- [71] S. Longhi, Topological Phase Transition in non-Hermitian Quasicrystals, Phys. Rev. Lett. **122**, 237601 (2019).
- [72] S. Longhi, Metal-insulator phase transition in a non-Hermitian Aubry-André-Harper model, Phys. Rev. B **100**, 125157 (2019).
- [73] T. Liu, H. Guo, Y. Pu, and S. Longhi, Generalized Aubry-André self-duality and mobility edges in non-Hermitian quasiperiodic lattices, Phys. Rev. B **102**, 024205 (2020).
- [74] Y. Liu, X.-P. Jiang, J. Cao, and S. Chen, Non-Hermitian mobility edges in one-dimensional quasicrystals with parity-time symmetry, Phys. Rev. B **101**, 174205 (2020).
- [75] Q. Zeng, Y. Yang, and R. Lü, Topological phases in one-dimensional nonreciprocal superlattices, Phys. Rev. B **101**, 125418 (2020).
- [76] Q. Zeng, Y. Yang, and Y. Xu, Topological phases in non-Hermitian Aubry-André-Harper models, Phys. Rev. B **101**, 020201(R) (2020).
- [77] L. Zhai, S. Yin, and G. Huang, Many-body localization in a non-Hermitian quasiperiodic system, Phys. Rev. B **102**, 064206 (2020).
- [78] Q. Zeng and Y. Xu, Winding numbers and generalized mobility edges in non-Hermitian systems, Phys. Rev. Research **2**, 033052 (2020).
- [79] S. Longhi, Phase transitions in a non-Hermitian Aubry-André-Harper model, Phys. Rev. B **103**, 054203 (2021).
- [80] Y. Liu, Y. Wang, Z. Zheng, and S. Chen, Exact non-Hermitian mobility edges in one-dimensional quasicrystal lattice with exponentially decaying hopping and its dual lattice, Phys. Rev. B **103**, 134208 (2021).
- [81] Y. Liu, Y. Wang, X. Liu, Q. Zhou, and S. Chen, Exact mobility edges, PT-symmetry breaking, and skin effect in one-dimensional non-Hermitian quasicrystals, Phys. Rev. B **103**, 014203 (2021).
- [82] Z. Xu and S. Chen, Dynamical evolution in a one-dimensional incommensurate lattice with PT symmetry, Phys. Rev. A **103**, 043325 (2021).
- [83] X. Cai, Boundary-dependent self-dualities, winding numbers, and asymmetrical localization in non-Hermitian aperiodic one-dimensional models, Phys. Rev. B **103**, 014201 (2021).
- [84] L. Tang, G. Zhang, L. Zhang, and D. Zhang, Localization and topological transitions in non-Hermitian quasiperiodic lattices, Phys. Rev. A **103**, 033325 (2021).
- [85] T. Liu, S. Cheng, H. Guo, and X. Gao, Fate of Majorana zero modes, exact location of critical states, and unconventional real-complex transition in non-Hermitian quasiperiodic lattices, Phys. Rev. B **103**, 104203 (2021).
- [86] L. Zhai, G. Huang, and S. Yin, Cascade of the delocalization transition in a non-Hermitian interpolating Aubry-André-Fibonacci chain, Phys. Rev. B **104**, 014202 (2021).
- [87] L. Zhou, Floquet engineering of topological localization transitions and mobility edges in one-dimensional non-Hermitian quasicrystals, Phys. Rev. Research **3**, 033184 (2021).
- [88] L. Zhou and W. Han, Non-Hermitian quasicrystal in dimerized lattices, Chinese Phys. B **30**, 100308 (2021).
- [89] Z.-H. Wang, F. Xu, L. Li, D. Xu, and B. Wang, Unconventional real-complex spectral transition and Majorana zero modes in nonreciprocal quasicrystals, Phys. Rev. B **104**, 174501 (2021).
- [90] Y. Liu, Q. Zhou, and S. Chen, Localization transition, spectrum structure, and winding numbers for one-dimensional non-Hermitian quasicrystals, Phys. Rev. B **104**, 024201 (2021).
- [91] X. Cai, Localization and topological phase transitions in non-Hermitian Aubry-André-Harper models with p-wave pairing, Phys. Rev. B **103**, 214202 (2021).
- [92] S. Longhi, Non-Hermitian Maryland model, Phys. Rev. B **103**, 224206 (2021).

- [93] A. P. Acharya, A. Chakrabarty, and D. K. Sahu, Localization, PT-Symmetry Breaking and Topological Transitions in non-Hermitian Quasicrystals, *Phys. Rev. B* **105**, 014202 (2022).
- [94] C. Yuce and H. Ramezani, Coexistence of extended and localized states in the one-dimensional non-Hermitian Anderson model, *Phys. Rev. B* **106**, 024202 (2022).
- [95] L. Zhou and Y. Gu, Topological delocalization transitions and mobility edges in the nonreciprocal Maryland model, *J. Phys.: Condens. Matter* **34**, 115402 (2022).
- [96] W. Han and L. Zhou, Dimerization-induced mobility edges and multiple reentrant localization transitions in non-Hermitian quasicrystals, *Phys. Rev. B* **105**, 054204 (2022).
- [97] L. Zhou and W. Han, Driving-induced multiple PT-symmetry breaking transitions and reentrant localization transitions in non-Hermitian Floquet quasicrystals, *Phys. Rev. B* **106**, 054307 (2022).
- [98] X. Xia, K. Huang, S. Wang, and X. Li, Exact mobility edges in the non-Hermitian  $t_1 - t_2$  model: Theory and possible experimental realizations, *Phys. Rev. B* **105**, 014207 (2022).
- [99] T. Liu and X. Xia, Real-complex transition driven by quasiperiodicity: A class of non-PT symmetric models, *Phys. Rev. B* **105**, 054201 (2022).
- [100] L. Zhai, G. Huang, and S. Yin, Nonequilibrium dynamics of the localization-delocalization transition in the non-Hermitian Aubry-André model, *Phys. Rev. B* **106**, 014204 (2022).
- [101] S. Longhi, Non-Hermitian topological mobility edges and transport in photonic quantum walks, *Opt. Lett.* **47**, 2951 (2022).
- [102] X. Cai, Localization transitions and winding numbers for non-Hermitian Aubry-André-Harper models with off-diagonal modulations, *Phys. Rev. B* **106**, 214207 (2022).
- [103] W. Chen, S. Cheng, J. Lin, R. Asgari, and X. Gao, Breakdown of the correspondence between the real-complex and delocalization-localization transitions in non-Hermitian quasicrystals, *Phys. Rev. B* **106**, 144208 (2022).
- [104] L.-M. Chen, Y. Zhou, S. A. Chen, and P. Ye, Quantum entanglement of non-Hermitian quasicrystals, *Phys. Rev. B* **105**, L121115 (2022).
- [105] L. Zhou, Non-Abelian generalization of non-Hermitian quasicrystals: PT-symmetry breaking, localization, entanglement, and topological transitions, *Phys. Rev. B* **108**, 014202 (2023).
- [106] S. Longhi, Phase transitions and bunching of correlated particles in a non-Hermitian quasicrystal, *Phys. Rev. B* **108**, 075121 (2023).
- [107] L. Zhou and D. Zhang, Non-Hermitian Floquet Topological Matter—A Review, *Entropy* **25**, 1401 (2023).
- [108] S. Weidemann, M. Kremer, S. Longhi and A. Szameit, Topological triple phase transition in non-Hermitian Floquet quasicrystals, *Nature (London)* **601**, 354 (2022).
- [109] Q. Lin, T. Li, L. Xiao, K. Wang, W. Yi, and P. Xue, Topological Phase Transitions And Mobility Edges in Non-Hermitian Quasicrystals, *Phys. Rev. Lett.* **129**, 113601 (2022).
- [110] In dimensionless units, the term  $2\pi\alpha$  can be viewed as a wavenumber. If  $\alpha$  takes a rational value  $p/q$ , with  $p$  and  $q$  being coprime integers, we have a crystal with the lattice period  $q$ , i.e.,  $\cos(2\pi\alpha(n+q)) = \cos(2\pi\alpha n)$  and  $\sin(2\pi\alpha(n+q)) = \sin(2\pi\alpha n)$  for our models. If  $\alpha$  takes an irrational value, we obtain a quasicrystal with no spatial periodicity. The value of  $\alpha$  then decides whether our models describe crystals or quasicrystals.
- [111] Eqs. (3) and (7) are conjectured forms of energy spectrum based on extended numerical calculations [68, 72, 79]. In the limit of large system size  $L \rightarrow \infty$ , one may view  $k$  as a synthetic quantum number of the spectrum.
- [112] Each value of  $\langle \text{Im}E \rangle$  is renormalized by the maximum of  $\langle \text{Im}E \rangle$  over the considered parameter space  $(J, V) \in [-2, 2] \times [-2, 2]$ , such that its range becomes  $[0, 1]$  in Figs. 1(a) and 1(c).
- [113] Let the hopping amplitude  $J$  be the unit of energy, the speed of excitation transport is around  $v \sim J$  in the extended phase [79]. The time span for excitations to propagate throughout the lattice of length  $L$  is  $t_c \sim L/v$ . The system is expected to reach the steady state when its evolution time  $T$  is larger than  $t_c$ .
- [114] J. Li, A. K. Harter, J. Liu, L. de Melo, Y. N. Joglekar, and L. Luo, Observation of parity-time symmetry breaking transitions in a dissipative Floquet system of ultracold atoms, *Nat. Commun.* **10**, 855 (2019).
- [115] F. Ferri, R. Rosa-Medina, F. Finger, N. Dogra, M. Soriente, O. Zilberberg, T. Donner, and T. Esslinger, Emerging Dissipative Phases in a Superradiant Quantum Gas with Tunable Decay, *Phys. Rev. X* **11**, 041046 (2021).
- [116] R. Rosa-Medina, F. Ferri, F. Finger, N. Dogra, K. Kroeger, R. Lin, R. Chitra, T. Donner, and T. Esslinger, Observing Dynamical Currents in a Non-Hermitian Momentum Lattice, *Phys. Rev. Lett.* **128**, 143602 (2022).
- [117] Z. Ren, D. Liu, E. Zhao, C. He, K. K. Pak, J. Li, and G.-B. Jo, Chiral control of quantum states in non-Hermitian spin-orbit-coupled fermions, *Nat. Phys.* **18**, 385 (2022).
- [118] Q. Liang, D. Xie, Z. Dong, H. Li, H. Li, B. Gadway, W. Yi, and B. Yan, Dynamic Signatures of Non-Hermitian Skin Effect and Topology in Ultracold Atoms, *Phys. Rev. Lett.* **129**, 070401 (2022).
- [119] N. Hatano and D. R. Nelson, Localization Transitions in Non-Hermitian Quantum Mechanics, *Phys. Rev. Lett.* **77**, 570 (1996).
- [120] J. Feinberg and A. Zee, Non-Hermitian localization and delocalization, *Phys. Rev. E* **59**, 6433 (1999).
- [121] K. Li, Z.-C. Liu, and Y. Xu, Disorder-Induced Entanglement Phase Transitions in Non-Hermitian Systems with Skin Effects, arXiv:2305.12342.
- [122] R. Hamazaki, K. Kawabata, and M. Ueda, Non-Hermitian Many-Body Localization, *Phys. Rev. Lett.* **123**, 090603 (2019).
- [123] K. Yamamoto and R. Hamazaki, Localization properties in disordered quantum many-body dynamics under continuous measurement, *Phys. Rev. B* **107**, L220201 (2023).
- [124] S. Li, X. Yu, and Z. Li, Emergent entanglement phase transitions in non-Hermitian Aubry-André-Harper chains, arXiv:2309.03546.